Solid Rocket Motor Combustion Instabilities: Analysis of the Transition to the First Limit Cycle

Giuseppe Lombardo and Vincenzo Oliveri

Dipartimento di Ingegneria Strutturale Aerospaziale e Geotecnica
Università degli Studi di Palermo, Facoltà di Ingegneria, Viale delle Scienze, Palermo 90128 Italy
e-mail: giuseppe.lombardo@unipa.it

Keywords: *solid, rocket, combustion, instability.*

Abstract. *A nonlinear multi time-scale analysis of the solid propellant rocket motor transition to the first limit cycle is presented and the motor behavior subsequent to some relevant transition scenarios is investigated. Important physical parameters characterizing the transition to limit cycle are then put in evidence and their cross-effects are studied. The analysis takes into account the effects of acoustic-vorticity-entropy wave coupling, waves steepening, rotational and viscous flow losses due to the steep-fronted waves, energy losses in the steepened state, nonlinear energy pathways and includes the study of the oscillatory energy losses in the nozzle, the unsteady combustion and the combustion chamber geometry changes resulting from the grain regression. The analysis provides evidence that in the investigated instability regions the wave amplitude evolution in the combustion chamber as well as the actual intrinsic motor stability is influenced by the time-history of selected parameter interactions.*

1 INTRODUCTION

When flow and combustion processes couple with the acoustic modes of the combustion chamber, solid propellant rocket motors (SRMs) experience unsteady gas motion, thrust oscillations and mechanical vibrations [1-9]. The acoustic oscillatory field interacting with the high energy densities of the combustion can be involved in a very rapid steepening process [10-14]. Damping process can limit the amplitude evolution of gas oscillations and the steepening of finite or high-amplitude pressure oscillations can terminate in shock-like oscillating structures similar to travelling shock waves. Noise processes can have effects on acoustic and finite amplitude oscillations growth. The role of non-linear processes in initiating and sustaining combustion instabilities has been and continues to be a subject of investigations. These analyses have yielded a great deal of insight into the complex non-linear behavior that is often observed in SRM combustion chambers and they have demonstrated the existence of stable limit cycles or the possibility of triggering instabilities in apparently stable motors [15-18]. The well-known limit cycle behavior in which the fluctuations keep their peak amplitude, the DC shift, an elevated increase in the mean chamber pressure and the triggering amplitude above which pulsing cause an apparently stable motor to transition to violent oscillations are examples of nonlinear effects of high-amplitude pressure oscillations in the SRM combustion chamber[19]. In this paper we want study the transition of a SRM to its first limit cycle (FLC) and we want investigate the motor behavior subsequent to some relevant transition scenarios. With this aim, we solve the SRM combustion instability problems adopting a nonlinear multi time-scale energy balance approach [19-21]. In the chamber model formulation, we include the equations of continuity, momentum, energy, state and species mass fraction and we introduce four time scales corresponding to the different dynamics of the phenomena involved in the combustion instabilities during the transition to the FLC. In particular, we take into account the effects of acoustic-vorticity-entropy wave coupling, of waves steepening, of rotational/viscous flow losses due to the steep-fronted waves, of intrinsic damping in the steepened state, of

nonlinear energy pathways, of unsteady combustion [22]. The model contemplate the physical parameters describing the operation of the SRM at its trigger limits and then in conditions ranging from high-amplitude longitudinal pressure oscillations in the combustion chamber to conditions lying in the FLC region [23-43]. The analysis can give a quantitative indication about the phenomena saturating the limit cycle such as nonlinear gasdynamics effects at high amplitudes of acoustic oscillations, nonlinear boundary conditions due to flow separation and nonlinear characteristics of the heat transfer process. It can be useful to outline the parameters characterizing the transition to the FLC, can furnish a nonlinear time-multi- scale mapping of the transition and the subsequent motor FLC. The study of some test cases can provide evidence that in the investigated instability regions the wave amplitude evolution in the combustion chamber is influenced by the time-history of some parameter interactions.

2 THE SRM MODEL

We introduce the following sets of dimensionless variables that are used for the formulation of the unsteady flow in the SRM combustion chamber.

$$\begin{cases} p = p^* / P_0 \\ \rho = \rho^* / \rho_0 \\ T = T^* / T_0 \\ \mathbf{u} = \mathbf{u}^* / a_0 \\ \mathbf{r} = \mathbf{r}^* / L \end{cases} \quad \begin{cases} \mathbf{F} = \mathbf{F}^* / (\rho_0 a_0^2 / L) \\ t = t^* / (L / a_0) \\ \boldsymbol{\omega} = \boldsymbol{\omega}^* / (a_0 / L) \\ e = e^* / a_0^2 \end{cases} \quad \begin{cases} w = w^* / (\rho_0 a_0 / L) = \text{Dimensionless reaction rate} \\ h_i^0 = (h_i^0)^* / a_0^2 = \text{Dimensionless heat of combustion} \\ Y_i = \text{Mass fraction for species\_}i \end{cases}$$

a_0 is the mean speed of sound, *L* is chamber length, $\mathbf{u}$ is unsteady velocity vector, t is the time, ρ_0 is the density; $\boldsymbol{\omega}$ is the unsteady vorticity amplitude. We denote with star (*) the dimensional quantities, with subscript zero (0), we indicate a quiescent and stabilized chamber reference condition. The Prandtl number Pr and the viscous reference lengths including dilatation and flame are

$$Pr \equiv \frac{c_p \mu}{\kappa} \qquad \delta^2 = \frac{\nu}{a_0 L} \qquad \delta_d^2 = \delta^2 \left(\eta / \mu + \frac{4}{3} \right) \qquad \delta_f \equiv \frac{\kappa}{\rho_0 c_p V} = \frac{\kappa}{\rho_0 c_p a_0 M_b}.$$

2.1 Governing Equations

In this section, we recall the equations of continuity, momentum, energy, state, and species mass fraction written using dimensionless variables and describing the unsteady flow in the SRM combustion chamber.

$$\frac{\partial \rho}{\partial t} + \nabla \cdot (\rho \mathbf{u}) = 0 \tag{1}$$

$$\rho \left(\frac{\partial \mathbf{u}}{\partial t} + \frac{1}{2} \nabla \mathbf{u} \cdot \mathbf{u} - \mathbf{u} \times \omega \right) = -\frac{1}{\gamma} \nabla p - \delta^2 \nabla \times \nabla \times \mathbf{u} + \delta_d^2 \nabla (\nabla \cdot \mathbf{u}) + \mathbf{F} \tag{2}$$

$$\begin{aligned} &\frac{\partial E}{\partial t} + \nabla \cdot \left[\rho \mathbf{u} \left(\frac{T}{\gamma(\gamma - 1)} + \frac{1}{2} \mathbf{u} \cdot \mathbf{u} \right) \right] = \frac{\delta^2}{(\gamma - 1) Pr} \nabla^2 T - \frac{1}{\gamma} \nabla \cdot (p \mathbf{u}) + \\ &+ \rho \mathbf{u} \cdot (\mathbf{u} \times \omega) + \mathbf{u} \cdot \mathbf{F} + \delta^2 \left[\omega \cdot \omega - \mathbf{u} \cdot \nabla \times \omega \right] + \delta_d^2 \left[(\nabla \cdot \mathbf{u})^2 + \mathbf{u} \cdot \nabla (\nabla \cdot \mathbf{u}) \right] - \sum_{i=1}^{N} h_i^0 w_i \end{aligned} \tag{3}$$

$$p_\chi = \rho_\chi T_\chi \tag{4}$$

$$\rho\left[\frac{\partial Y_i}{\partial t}+\mathbf{u}_\chi\cdot\nabla Y_i\right]-\frac{\delta^2}{Pr}\nabla^2 Y_i=w_{\chi i} \tag{5}$$

Where

$$E\equiv\rho\left(\frac{T}{\gamma(\gamma-1)}+\frac{1}{2}\mathbf{u}\cdot\mathbf{u}\right) \tag{6}$$

is the system energy density.

2.2 Time Varying Mean Flow Parameters

The oscillatory part of the flow variables is separated from the time-varying mean component by writing:

$$\begin{cases}\rho=\bar{\rho}+\rho^{(1)}\\ p=\bar{P}+p^{(1)}\\ T=\bar{T}+T^{(1)}\end{cases}\qquad\begin{cases}\mathbf{u}=\bar{M}_b\mathbf{U}+\mathbf{u}^{(1)}\\ \boldsymbol{\omega}=\bar{M}_b\nabla\times\mathbf{U}+\nabla\times\mathbf{u}^{(1)}=\bar{M}_b\boldsymbol{\Omega}+\boldsymbol{\omega}^{(1)}\end{cases} \tag{7}$$

The superscript (1) denotes the first-order accuracy in the amplitude of the oscillatory part of the variables in the time scale θ. The mean variables $\bar{\rho},\bar{P},\bar{T},\bar{M}_b$ are strongly influenced by the transition to the FLC in the time scale χ. They are also functions of non-oscillatory dynamics as the pressure DC shift dynamics that develops in the time scale τ and they depend on the changes in the chamber geometry consequent to the grain regression in the time scale σ. In what follow, we intrinsically consider $\bar{\rho}=\bar{\rho}(\theta,\chi,\tau,\sigma)$, $\bar{p}=\bar{p}(\theta,\chi,\tau,\sigma)$, $\bar{T}=\bar{T}(\theta,\chi,\tau,\sigma)$, $\bar{M}_b=\bar{M}_b(\theta,\chi,\tau,\sigma)$.

The time-depending amplitude of the oscillatory part of the variables is factored out by defining primed variables. For example, for the oscillatory pressure we write

$$p^{(1)}=\varepsilon(t)\,p' \tag{8}$$

2.3 Energy Balance

Using Eq. (7), expanding and time averaging the equation of energy Eq. (3) it is possible to obtain the equation for the system amplitude.

$$\frac{d\varepsilon}{dt}=\frac{\left[\left\langle\begin{array}{c}-\nabla\cdot\left[\rho\mathbf{u}\left(\frac{T}{\gamma(\gamma-1)}+\frac{1}{2}\mathbf{u}\cdot\mathbf{u}\right)\right]+\frac{\delta^2}{(\gamma-1)Pr}\nabla^2T-\frac{1}{\gamma}\nabla\cdot(p\mathbf{u})\\ +\rho\mathbf{u}\cdot(\mathbf{u}\times\omega)+\delta^2\left[\omega\cdot\omega-\mathbf{u}\cdot\nabla\times\omega\right]+\delta_d^2\left[\mathbf{u}\cdot\nabla(\nabla\cdot\mathbf{u})+(\nabla\cdot\mathbf{u})^2\right]-\sum_{i=1}^{N}h_i^0w_i\end{array}\right\rangle\right]_\chi}{2\varepsilon\frac{1}{\gamma\bar{P}}\left[\left\langle\left(\frac{p'}{\gamma}\right)^2\right\rangle+\frac{1}{2}\bar{\rho}\langle\mathbf{u}'\cdot\mathbf{u}'\rangle\right]} \tag{9}$$

Where we recognize

$$\frac{1}{\gamma \bar{P}}\left\langle \left(\frac{p'}{\gamma}\right)^2 \right\rangle + \frac{1}{2}\bar{\rho}\left\langle u' \cdot u' \right\rangle = \left\langle E \right\rangle \tag{10}$$

the time-averaged oscillatory energy. Integrating the time-averaged energy density over the chamber control volume, we obtain the system energy

$$E^2 \equiv \iiint_V \frac{1}{\gamma \bar{P}}\left\langle \left(\frac{p'}{\gamma}\right)^2 \right\rangle + \frac{1}{2}\bar{\rho}\left\langle u' \cdot u' \right\rangle dV \tag{11}$$

and the rate of change of system amplitude can be written in the form:

$$\frac{d\varepsilon}{dt} = \alpha^{(1)}\varepsilon + \alpha^{(2)}\varepsilon^2 + \alpha^{(3)}\varepsilon^3 + \alpha^{(4)}\varepsilon^4 \tag{12}$$

the coefficients of this non linear differential equation can be written as

$$\begin{aligned} \alpha_\chi^{(1)} = \frac{1}{2\gamma^2 E_\chi{}^2}\Bigg\{ & \iint_{S_b} \left(\bar{M}_b\right)_\chi \left(A_b^{(r)} + \frac{1}{\gamma \bar{P}_\chi} \right) \left\langle p'^2 \right\rangle dS - \iint_{(S_N)_\chi} \left(\bar{M}_N\right)_\chi \left(\left(A_N^{(r)}\right)_\chi + \frac{1}{\gamma \bar{P}_\chi} \right) \left\langle p'^2 \right\rangle dS \\ & + \iint_{S_b^=} \left(\bar{M}_b\right)_\chi \left\langle p'^2 \right\rangle dS - \iint_{S_b^=} \left(\frac{\delta}{2\left(\bar{M}_b\right)_\chi} \right)^2 \left\langle \nabla p' \cdot \nabla p' \right\rangle dS \end{aligned} \tag{13}$$

$$\alpha_\chi^{(2)} = \frac{\pi}{2\gamma^2 E_\chi{}^2}\left(\frac{\gamma+1}{12\gamma}\right) \tag{14}$$

$$\alpha^{(3)} = \frac{1}{2\mathrm{E}^2}\iiint_{\mathrm{V}} \left\langle \begin{array}{l} -\left(\frac{1}{2}u' \cdot u'\right)\left(\nabla \cdot \rho' u'\right) - \mathrm{a}_3 u' \cdot \nabla\left(\frac{\rho'}{\bar{\rho}}\right)^3 \\ -\rho' u' \cdot \left[\frac{1}{2}\nabla\left(u' \cdot u'\right) - u' \times \omega'\right] \end{array} \right\rangle \mathbf{dV} + \frac{3\pi}{4\mathrm{E}^2}\left(\frac{\gamma+1}{12\gamma^3}\right) \tag{15}$$

$$\alpha^{(4)} = -\frac{3\pi}{40\mathrm{E}}\left(\frac{\gamma+1}{12\gamma^3}\right)\left(\frac{11\gamma^2+1}{\gamma^2}\right) \tag{16}$$

Retaining non linear terms in expanding the continuity equation, Eq. (1), taking the time average and integrating over the chamber volume, the equation for the rate of change of the chamber operating pressure can be written

$$\frac{d\bar{P}}{dt} = \left\{ -\frac{1}{V}\iint_S n \cdot \left(\bar{\rho}\bar{M}_b U\right) dS - \varepsilon^2 \left(\frac{1}{\gamma \bar{V}}\right) \iint_S n \cdot \left\langle p^{(1)} u^{(1)} \right\rangle dS \right\} \tag{17}$$

An expanded form is given by

$$\frac{d\bar{P}}{dt} = \varphi_\chi \bar{P}^n + \eta_\chi \bar{P} + \beta_\chi^{(2)} \varepsilon^2 \tag{18}$$

where the first two terms φ_χ and η_χ term are handled by means of the unsteady internal ballistics calculations for the solid rocket motor and $\beta_\chi^{(2)}$ is the term that leads to the mean pressure shift.

An expanded expression for this term is:

$$\beta_\chi^{(2)} = \frac{1}{2\gamma^2 V} \iint_{S_b} \left(\bar{M}_b\right)_\chi \left(A_b^{(r)} + 1\right) \left\langle p'^2 \right\rangle dS \tag{19}$$

2.4 Unsteady combustion

The unsteady-state model is based on a steady-state description derived from physical principles and it developed using a direct simulation approach. It includes some additional terms to account for thermal lags and conductive "capacitance" in the solid phase. The steady-state model is a separate-surface-temperature model with a heterogeneous flame structure including deflagration, reaction diffusion flames written for mono-modal AP/HTPB propellants. A coordinate system is defined as 0 at the surface, +∞ high above the surface, and −∞ far below the surface.

Equations for oxidizer mass flux, binder mass flux, total mass flux, height of pre-mixed (AP) flame, height of reaction flame, height of diffusion flame, height of total flame, surface temperature of binder, surface temperature of oxidizer, and pre-mixed flame temperature are involved.

The mass fluxes can be obtained by Arrenius expressions

$$\dot{m}_{ap} = A_{s,ap} \exp\left(-\frac{E_{s,ap}}{RT_{s,ap}}\right) \quad \dot{m}_b = A_{s,b} \exp\left(-\frac{E_{s,b}}{RT_{s,b}}\right) \quad \dot{m}_p = \alpha_{ap} \frac{\rho_p}{\rho_{ap}} \dot{m}_{ap} + \left(1-\alpha_{ap}\right) \frac{\rho_p}{\rho_b} m_b \tag{20}$$

$A_{s,ap}$ is a constant referred to the surface of AP, $E_{s,ap}$.is the activation energy, R is the universal gas constant, $T_{s,ap}$ is the surface of AP temperature, $A_{s,b}$ is a constant referred to the surface of binder, $E_{s,b}$ is the activation energy, $T_{s,b}$ is the surface of binder temperature, α_{ap} is the mass fraction of the AP, ρ_{ap} is the AP density, ρ_p is the total propellant density, ρ_b is the binder density.

The flame heights can be expressed by

$$x_{f,ap} = \frac{\dot{m}_{ap}}{P^2 A_{g,ap} \exp\left(-\frac{E_{g,ap}}{RT_{f,ap}}\right)} \qquad x_r = \frac{\dot{m}_p}{P^2 A_r \exp\left(-\frac{E_r}{RT_f}\right)} \qquad x_d = \left(\frac{\dot{m}_p D_{ap}^{*2}}{A_{diff}\left(\rho_g D_g\right)_{eff}}\right) \tag{21}$$

Energy balances from far below the surface to just above the surface provides equations for the surface temperatures of the AP and binder and the energy balance in the AP can be written

$$\dot{m}_{ap} C_{p,or,ap} T_i + \lambda_{g,ap} \left.\frac{\partial T}{\partial x}\right|_{x=0^+} + \dot{m}_{ap} Q_{v,ap} = \dot{m}_{ap} C_{p,g,ap} T_{s,ap} + \int_{-\infty}^{0} \rho C_p \frac{\partial T}{\partial t} \partial x \tag{22}$$

The energy balance in the binder can have a similar form.

Eq. (22) and the similar one corresponding to the binder are handled by using FEM in space and FDM in time.

2.5 Nozzle admittance

The wave pattern inside the chamber depends upon the interaction of the incident wave and the reflected wave from the nozzle, which in turn depends upon the amplitude and phase changes. We define the nozzle admittance using two parameters, α and β, the sound pressure in the chamber, the Mach number, the frequency and the velocity of sound. The amplitude change upon reflection is a function of α whereas the phase change is a function of β. The ratio of the reflected amplitude P_R to the incident amplitude P_I at the location where admittance is measured is given by $\frac{P_R}{P_I} = e^{-2\pi\alpha}$, a similar relationship for the sound energy, W, is given by $\frac{W_R}{W_I} = e^{-4\pi\alpha}$ and the phase change upon reflection is expressed by $\theta = \pi(1+2\beta)$. The values of α and β are determined with the aid of the following expression that describes the behaviour of the wave pattern inside the chamber:

$$\left|p(z,r,\theta)\right| = P_0\left[J_m(S_{mn})\right]\cos(m\theta)\left\{\cosh^2\alpha - \cos^2\left[\pi\left(\beta + \frac{2d}{\lambda}\right)\right]\right\}^{\frac{1}{2}} \tag{23}$$

In this equation $\left|p(z,r,\theta)\right|$ is the magnitude RMS of the pressure at the point z, r, θ, while P_0 is the amplitude RMS of the pressure oscillation at the end of the chamber. λ is the wavelenght, d is the distance from the nozzle entrance, S_{mn} is the transverse mode eigenvalue of the Bessel function of first kind of order m, $J_m(x)$.

In Eq. (23) P_0, α and β can be determined by three pressure measurements at different axial positions, the angular frequency $s = 2\pi f \frac{r_c(x)}{c}$ is the independent variable with f frequency of oscillation, $r_c(x)$ characteristic length of the chamber and c speed of sound in the chamber. Once the parameters α and β have been determined, they are used to determine the nozzle admittance of a single wave $\tilde{A}_n$, which is given by the relationship $\tilde{A}_n = \frac{g}{\rho c}\left(\frac{a}{b}\right)(\Gamma + i\eta)$ where $a = \frac{\omega}{c}\sqrt{\left(\frac{\omega}{c}\right)^2 - \left(\frac{S_{mn}}{r_c(x)}\right)^2(1-M^2)}$,

$b = \left(\frac{\omega}{c}\right)^2 + \left(\frac{S_{mn}}{r_c(x)}M\right)^2$, $\Gamma = \frac{\tanh(\pi\alpha)\sec^2(\pi\beta)}{\tanh^2(\pi\alpha)+\tan^2(\pi\beta)} + \frac{1}{a}\left(\frac{S_{mn}}{r_c(x)}\right)^2 M$, $\eta = \frac{\sec h^2(\pi\alpha)\tan(\pi\beta)}{\tanh^2(\pi\alpha)+\tan^2(\pi\beta)}$ and M is the mean chamber Mach number. The nozzle acoustic admittance consequent to all the waves that cross the nozzle entrance surface σ can be expressed by $A_n = \iint_\sigma \sum_\lambda \tilde{A}_n$ where $\sum_\lambda \tilde{A}_n$ indicates the wave path of a single wave crossing the σ surface. The nozzle convergent geometry is implicitly expressed in the $\sum_\lambda$ operator.

3 TRANSITION SIMULATIONS

We analyze the transition of the solid propellant rocket motor to its FLC and we investigate the motor behavior subsequent to some relevant transition scenarios, performing the transition calculation applied on a solid rocket motor with a circular cylindrical chamber and with aspect ratio and propellant characteristics typical of a tactical motor. We accurately determine the stability coefficients in terms of the actual system

parameters and geometry. Nozzle admittance, propellant admittance, grain regression and unsteady burning calculations are included. We analyze nineteen different transition scenarios. All of them are triggered by a pulse fired at the instant of the motor operation time when the grain thickness is reduced to 10 mm. For each scenario, we calculate and plot during the entire motor operation time the value of the chamber pressure, the wave amplitude, the mean chamber pressure, the mass flow rate, the Mach number at the burning surface, the mean wave amplitude, and the stability coefficients. The scenarios studied include the analysis of the effects of changes in burning rate, burning rate exponent, temperature coefficient, propellant density, aspect ratio, stability coefficients and their parts via the involved physical parameters, nozzle and propellant admittances, system energy density, time average of square of primed variable (defined by factoring out slowly changing amplitude) representative of steepened state.

4 RESULTS AND DISCUSSION

To keep the limit of the paper we present and discuss in detail only a little part of the FLC transition simulation we have performed for the pulsed tactical motor discussed above. A more general and comprehensive result discussion is given in concluding remarks section.

Of the nineteen parameters studied in the analysis, those that mostly influence the behavior of the motor are the burning rate, the burning rate exponent, the temperature coefficient, α_1 and α_2. The pressure in combustion chamber corresponding to the increase of each single parameter results always increase, except for the increasing of the coefficient α_2. Corresponding to the increase of this parameter in fact, as it is possible to see from the Fig. 5, the pressure in the chamber dwells to values always lower and shows a smaller DC shift. More complex it is the variation of the wave amplitude. The stability coefficients are influenced in various ways by the parameters in study, nevertheless the value limiting the acoustic energy results to be decreasing for increasing of the burning rate, of the temperatures coefficient and of the coefficient α_2. Increasing the burning rate, α_1 decreases and α_2 increases. Increasing the temperatures coefficient, α_2 shift decrease sensibly, but the behavior after shows a greater growth. The value limiting the acoustic energy decreases always. In the opposite as it is possible to not from Fig 2 and 3, it increases with increasing α_1, while it is quite resulting not influenced by the burning rate exponent changes.

4.1 Burning rate scenario

Fig. 1 shows the results of the transition simulation for the burning rate scenario. It is possible to observe that increasing the burning rate, the transition occurs earlier and shows higher DC shift; the mean pressure before the transition increases; after the transition increases with higher rate; the pressure oscillations increase sensibly; the wave amplitude peaks decrease; the Mach number shows no relevant changes; during the transition, α_1 shifts increase and after the transition α_1 decrease more rapidly; α_2 shifts decrease and after the transition α_2 increase more rapidly; β_2 shifts decrease and slow, after the transition β_2 decrease with higher rate.

4.2 Burning rate exponent scenario

Fig. 2 shows the results of the transition simulation for the burning rate exponent scenario. It is possible to observe that increasing the burning rate exponent, the transition occurs a little earlier and shows a little higher DC shift; the mean pressure before the transition increases; after the transition increases with a little higher rate; the pressure oscillations increase sensibly; the wave amplitude peaks decrease a little; the Mach number shows no relevant changes; during the transition, α_1 shifts shows no relevant changes, before the transition the effects are little and after the transition α_1 decrease is more slow; α_2 shifts shows no relevant changes, before the transition α_2 increase more slowly and after the transition α_2 increase more rapidly; β_2 shows no relevant changes.

4.2 α_1 scenario

Fig. 4 shows the results of the transition simulation for the α_1 scenario. It is possible to observe that increasing α_1, the transition occurs a little earlier and shows increases in DC shift; the mean pressure before and after the transition shows no changes; the pressure oscillations increase; the wave amplitude peaks increase; the Mach number shows no relevant changes; during the transition, α_2 shifts increases and became more sharp, before and after the transition α_2 increase more rapidly; β_2 shows no relevant changes.

5 CONCLUDING REMARKS

An analysis of the SRM transition to FLC adopting a nonlinear multi time-scale energy balance approach has been presented. The chamber model formulation includes models for unsteady burning, nozzle admittance, propellant admittance and grain regression. We introduce four time scales corresponding to the different dynamics of the phenomena involved in the combustion instabilities linked to the transition to the FLC. We use the time scale θ related to the instability oscillations, the time scale χ associated with the transition to the FLC, the time scale τ linked to the slower changing phenomena connected with the evolution of the instabilities (non-oscillatory parameters values or the pressure DC shift), the time scale σ related to changes in the geometries of the chamber consequent to the grain regression. We take into account the mentioned phenomena and their interactions simultaneously. In particular, we include the effects of acoustic-vorticity-entropy wave coupling, of waves steepening, of rotational/viscous flow losses due to the steep-fronted waves, of intrinsic damping in the steepened state, of nonlinear energy pathways. The motor model explicitly takes into account the coupling of the transient effects in the chamber flow and the unsteady combustion subsequent to the transition to the FLC with the acoustic, vorticity and entropy oscillations that the SRM can sustain and allows the simulation of the motor operation in a wide region of its FLC. With the example results presented, we are able to note that the motor behavior after the transition to the FLC changes depending on the operating point of the motor in which the transition occurs: the operating point values and the motor steady or transient operating condition. We note also that the instability dynamics after the transition are influenced by the dynamics in the time scale χ. In other words, under the same global conditions, to a specific transition corresponds a specific FLC, and in general, for the matching of the physical parameters involved in the time scale χ, the transition affects the evolution of the instability phenomena also in the other time scales. The time-history and time-scale influences discussed above open the perspective of a new concept of affecting the wave amplitude evolution. The management of the wave amplitude evolution in instability regions could enable the opportunity to enlarge the operational limits of the solid rocket motor. Moreover, it could also contribute to the development of a motor-level insensitivity to some external shocks strong enough to induce high-amplitude combustion chamber pressure fluctuations or able to cause combustion instability.

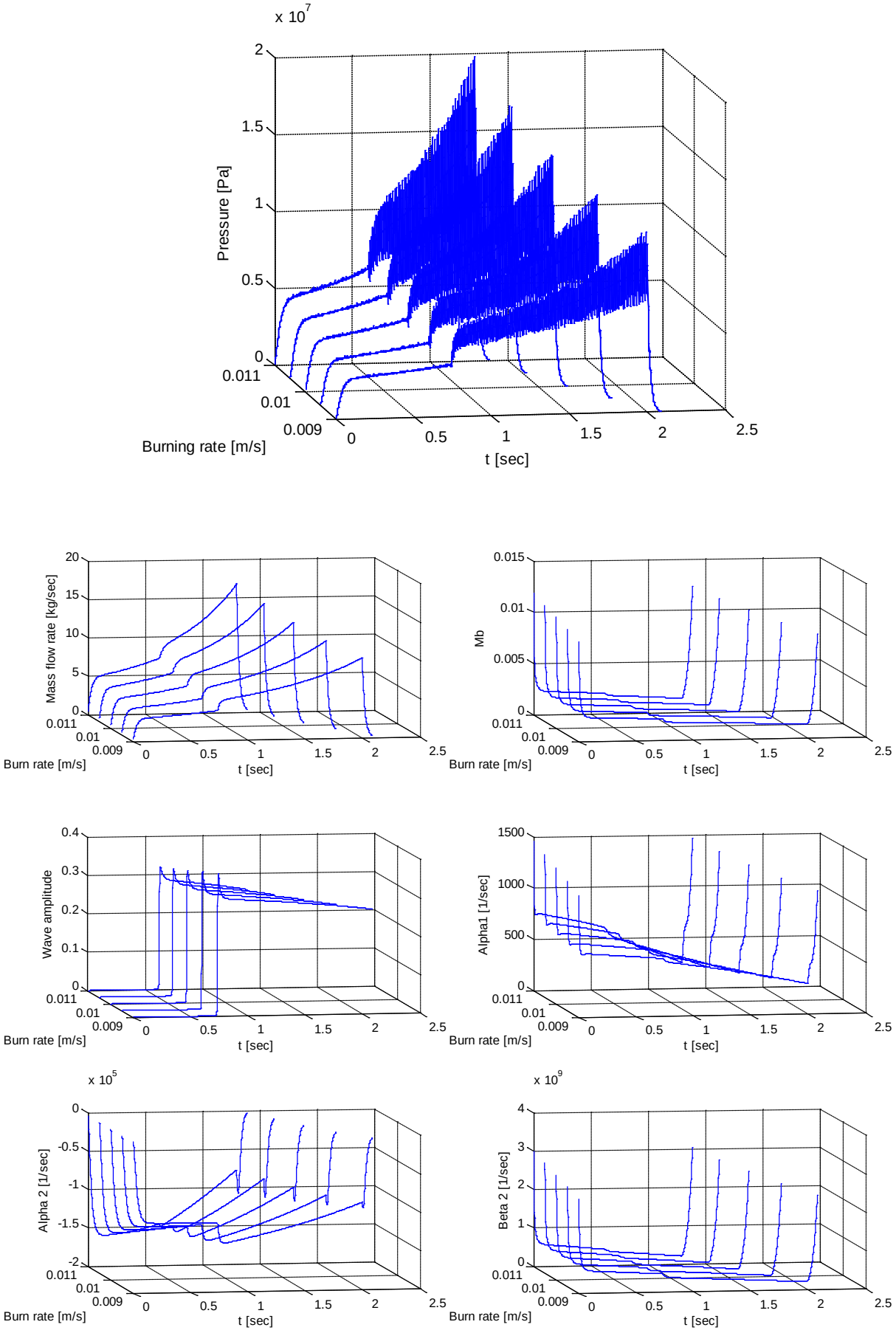

Figure 1: Pulsed tactical motor FLC transition. *Chamber pressure, mass flow rate, Mach number at the burning surface, wave amplitude, and stability coefficients in burning rate scenario.*

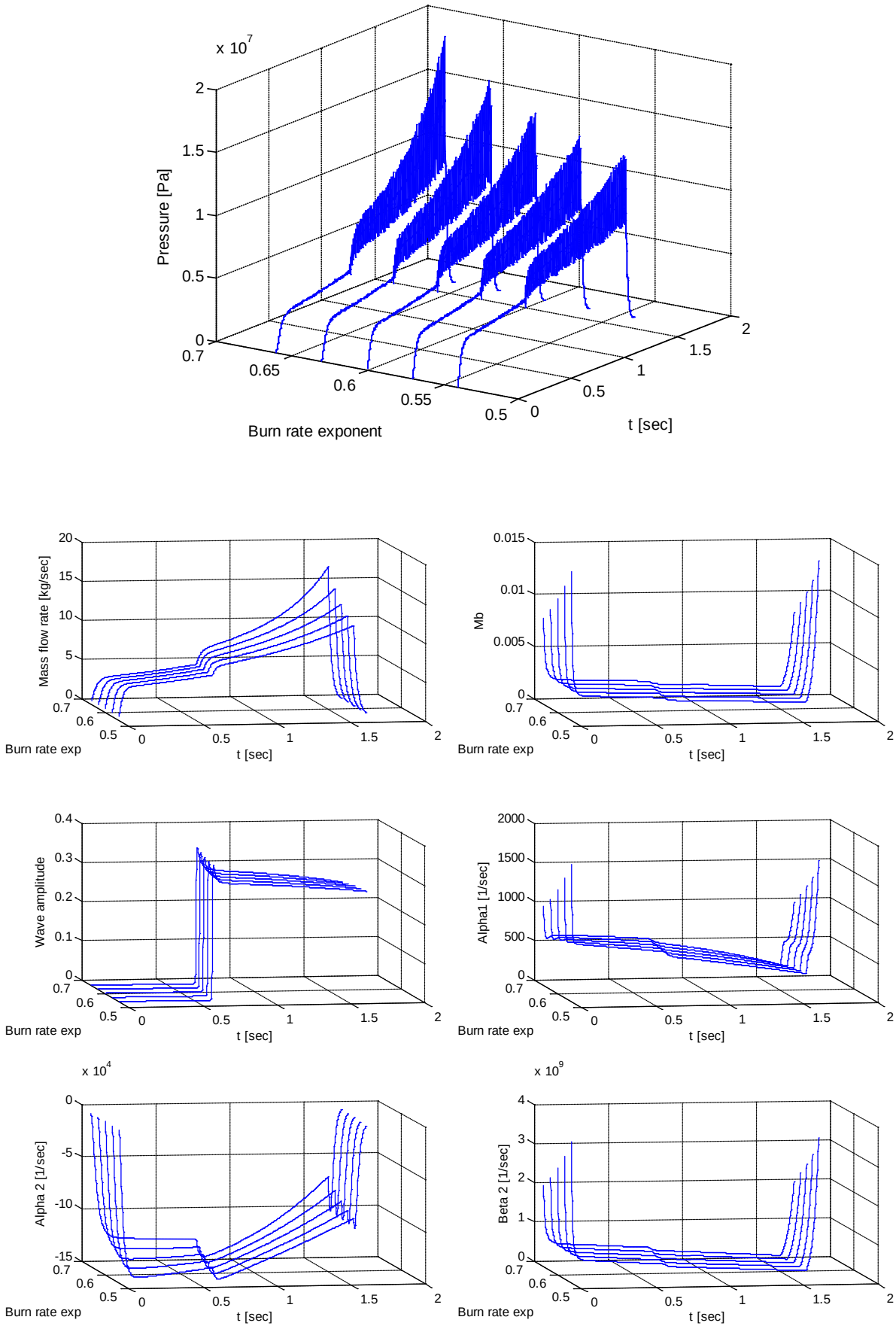

Figure 2: Pulsed tactical motor FLC transition. *Chamber pressure, mass flow rate, Mach number at the burning surface, wave amplitude, and stability coefficients in burn rate exponent scenario.*

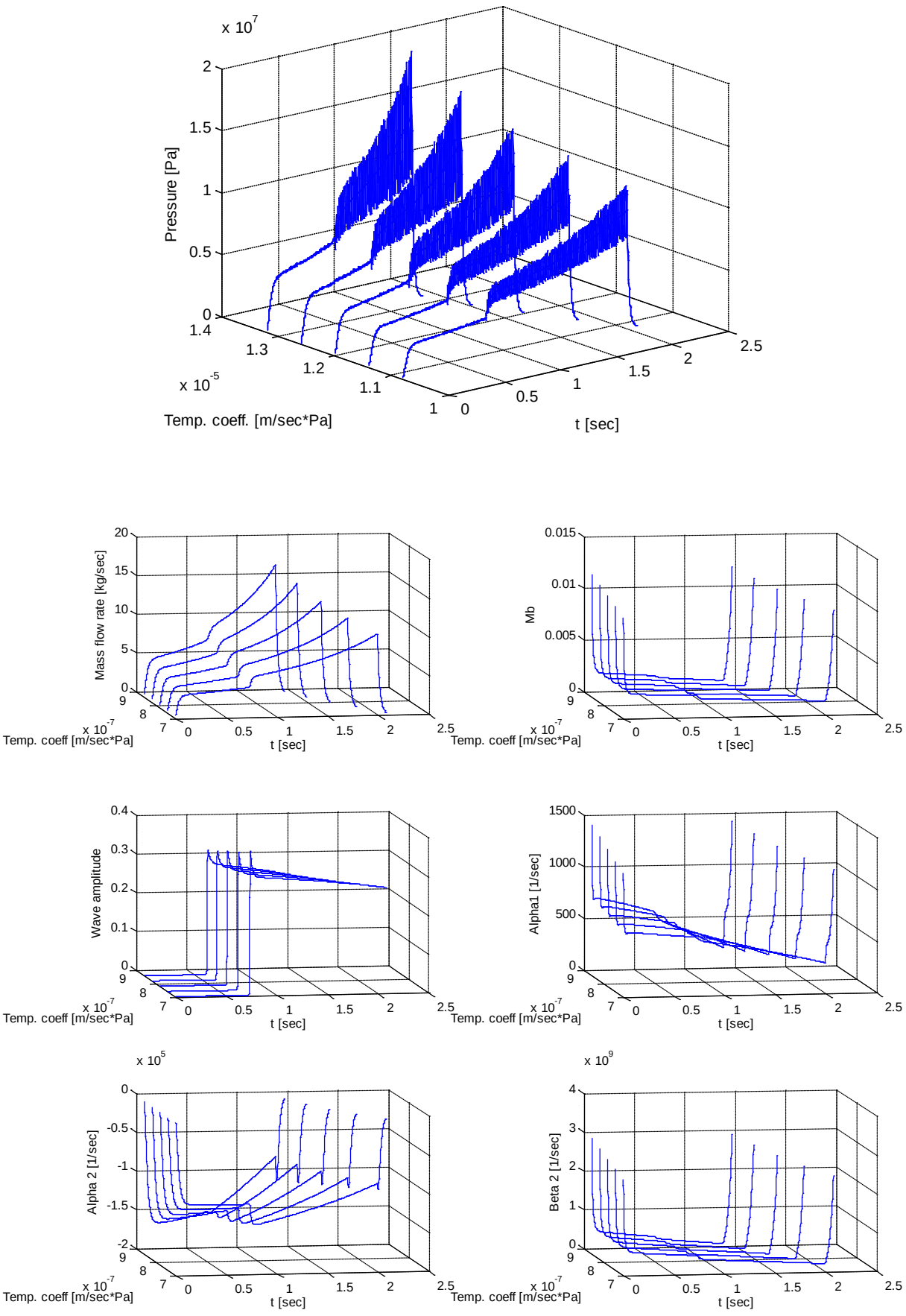

Figure 3: Pulsed tactical motor FLC transition. *Chamber pressure, mass flow rate, Mach number at the burning surface, wave amplitude, and stability coefficients in temperature coefficient scenario.*

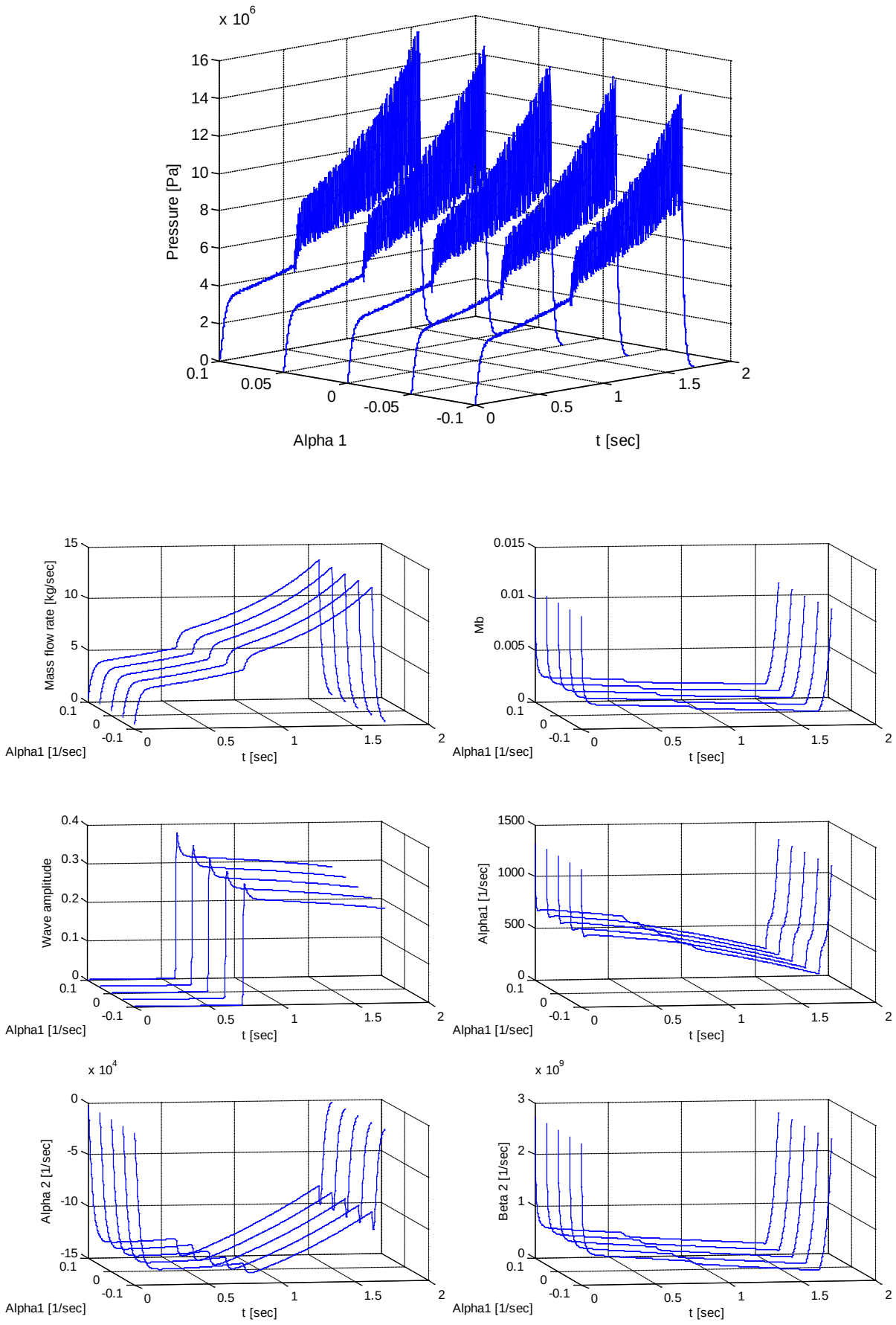

Figure 4: Pulsed tactical motor FLC transition. *Chamber pressure, mass flow rate, Mach number at the burning surface, wave amplitude, and stability coefficients in* α_1 *scenario.*

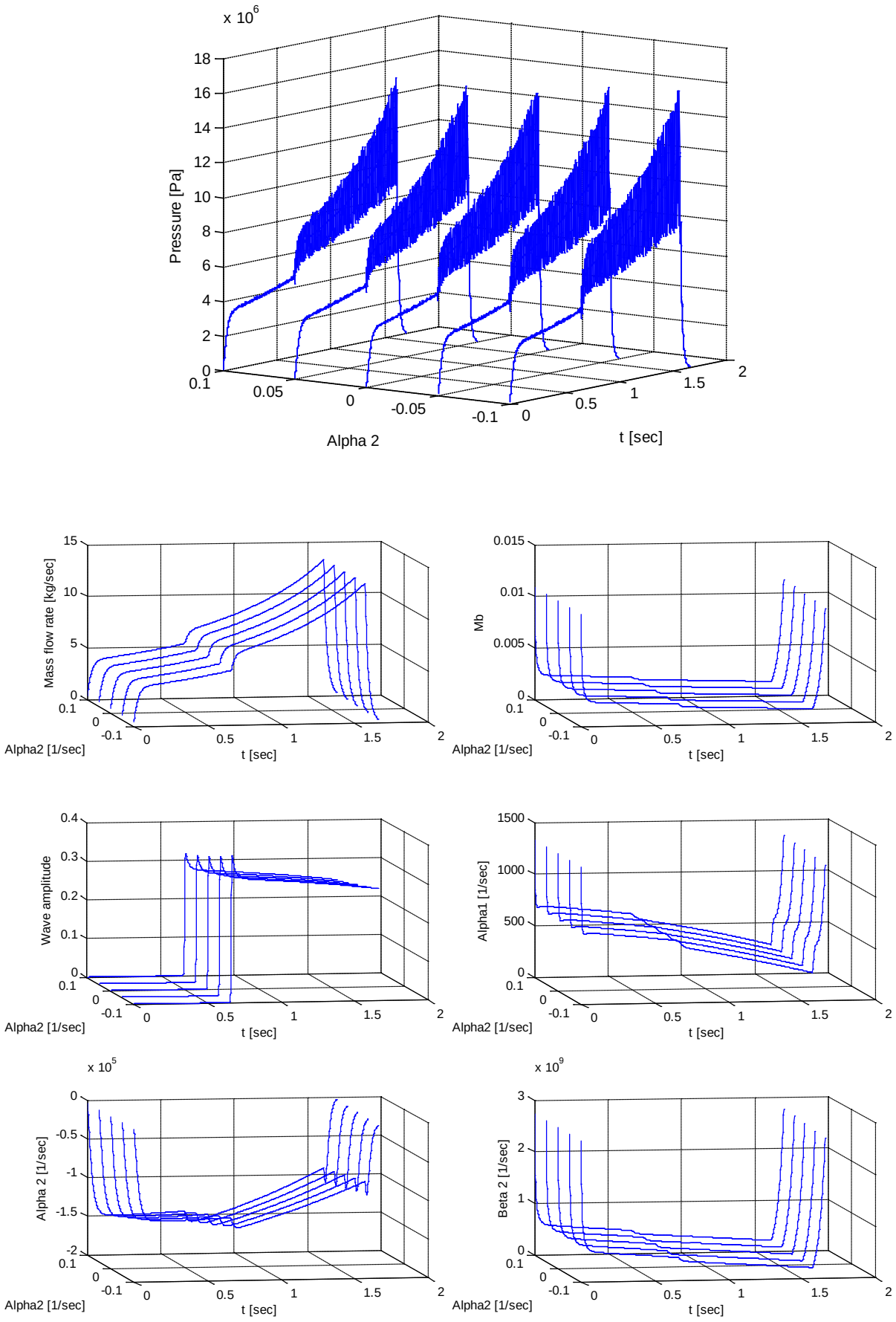

Figure 5: Pulsed tactical motor FLC transition. *Chamber pressure, mass flow rate, Mach number at the burning surface, wave amplitude, and stability coefficients in* α_2 *scenario.*

References

[1] Hart, R. W., and McClure, F. T., "Combustion Instability: Acoustic Interaction with a Burning Propellant Surface," *The Journal of Chemical Physics,* Vol. 10, No. 6, 1959, pp. 1501-1514.

[2] Roh, T. S., Tseng, I. S., and Yang, V., "Effects of Acoustic Oscillations on Flame Dynamics of Homogeneous Propellants in Rocket Motors," *Journal of Propulsion and Power,* Vol. 11, No. 4, 1995, pp. 640-650.

[3] Culick, F. E. C., "Acoustic Oscillations in Solid Propellant Rocket Chambers," *Acta Astronautica,* Vol. 12, No. 2, 1966, pp. 113-126.

[4] Shusser, M., Culick, F. E. C., Cohen, N. S., "Analytical Solution for Pressure-Coupled Combustion Response Functions of Composite Solid Propellants," *Journal of Propulsion and Power*, Vol. 24, No. 5, 2008, pp. 1058-1067.

[5] Flandro, G. A., and Majdalani, J., "Aeroacoustic Instability in Rockets," *AIAA Journal,* Vol. 41, No. 3, 2003, pp. 485-497.

[6] Yang, V., Wicker, J., and Yoon, M. W., "Acoustic Waves in Combustion Chambers," *Liquid Rocket Engine Combustion Instability*, Vol. 169, edited by V. Yang and W. E. Anderson, AIAA Progress in Astronautics and Aeronautics, 1995, pp. 357-376.

[7] Hart, R. W., and McClure, F. T., "Theory of Acoustic Instability in Solid Propellant Rocket Combustion," *Tenth Symposium (International) on Combustion*, 1964, pp. 1047-1066.

[8] Culick, F. E. C., "Some Recent Results for Nonlinear Acoustics in Combustion Chambers," *AIAA Journal*, Vol. 32, No. 1, 1994, pp. 146-168.

[9] Culick, F. E. C., "Combustion Instabilities in Propulsion Systems," *American Society of Mechanical Engineers, Noise Control and Acoustics Division,* Vol. 4, 1989, pp. 33-52.

[10] Culick, F. E. C., "Nonlinear Behavior Acoustic Waves in Combustion Chambers, Parts 1 and 2," *Acta Astronautica,* Vol. 3, 1976, pp. 714-757.

[11] Brownlee, W. G., "Nonlinear Axial Combustion Instability in Solid Propellant Motors," *AIAA Journal,* Vol. 2, No. 2, 1964, pp. 275-284.

[12] Brownlee, W. G., and Marble, F. E., "An Experimental Investigation of Unstable Combustion in Solid Propellant Rocket Motors," *ARS Progress in Astronautics and Rocketry: Solid Propellant Rocket Research*, Vol. 1, edited by M. Summerfield, Academic Press Inc., New York, 1960, pp. 455- 494.

[13] Blomshield, F. S., Crump, J. E., Mathes, H. B., Stalnaker, R. A., and Beckstead, M. W., "Stability Testing of Full-Scale Tactical Motors," *Journal of Propulsion and Power*, Vol. 13, No. 3, 1997, pp. 349-355.

[14] Blomshield, F. S., Mathes, H. B., Crump, J. E., Beiter, C. A., and Beckstead, M. W., "Nonlinear Stability Testing of Full-Scale Tactical Motors," *Journal of Propulsion and Power*, Vol. 13, No. 3, 1997, pp. 356-366.

[15] Flandro, G. A., "Approximate Analysis of Nonlinear Instability with Shock Waves," AIAA Paper 82-1220, July 1982.

[16] Vuillot, F., and Avalon, G., "Acoustic Boundary Layer in Large Solid Propellant Rocket Motors Using Navier-Stokes Equations," *Journal of Propulsion and Power,* Vol. 7, No. 2, 1991, pp. 231-239.

[17] Brownlee, W. G. and. Kimball., G H, "Shock Propagation in Solid-Propellant Rocket Combustors," *AIAA*, Vol. 4, No. 6, 1966, pp. 1132-1134.

[18] Vuillot, F., "Numerical Computation of Acoustic Boundary Layers in Large Solid Propellant Space Booster," AIAA Paper 91-0206, January 1991.

[19] Flandro, G. A., Fischbach, S. R., Majdalani, J., and French, J. C., "Nonlinear Rocket Motor Stability Prediction: Limit Amplitude, Triggering, and Mean Pressure Shift," AIAA Paper 2004-4054, July 2004.

[20] Lombardo, G., "Controllable Solid Propellant Rocket Motor Stability: Deep and Rapid Variable Thrust Operations," AIAA Paper 2008-4608, July 2008.

[21] Lombardo, G., "Liquid Aluminum Particle Effects on Propagation of Waves in solid rocket motor internal flow," 2nd EUCASS (European Conference For Aerospace Sciences), July 1-6, 2007.

[22] Lombardo, G., Oliveri, V., "Propellant Non-Steady Burning Effects on Controllable Solid Rocket Motor Internal Ballistic" XX AIDAA Congress, June 29, 2009.

[23] Culick, F. E. C., "Combustion Instabilities: Mating Dance of Chemical, Combustion, and Combustor Dynamics," AIAA Paper 2000-3178, July 2000.

[24] Culick, F. E. C., "Stability of Longitudinal Oscillations with Pressure and Velocity Coupling in a Solid Propellant Rocket," *Combustion Science and Technology,* Vol. 2, No. 4, 1970, pp. 179-201.

[25] Culick, F. E. C., "Stability of Three-Dimensional Motions in a Rocket Motor," *Combustion Science and Technology,* Vol. 10, No. 3, 1974, pp. 109-124.

[26] Culick, F. E. C., "The Stability of One-Dimensional Motions in a Rocket Motor," *Combustion Science and Technology,* Vol. 7, No. 4, 1973, pp. 165-175.

[27] Chedevergne, F., and Casalis, G., "Detailed Analysis of the Thrust Oscillations in Reduced Scale Solid Rocket Motors," AIAA Paper 2006-4424, July 2006.

[28] Chedevergne, F., and Casalis, G., "Thrust Oscillations in Reduced Scale Solid Rocket Motors, Part II : A New Theoretical Approach," AIAA Paper 2005-4000, July 2005.

[29] Chedevergne, F., Casalis, G., and Féraille, T., "Biglobal Linear Stability Analysis of the Flow Induced by Wall Injection," *Physics of Fluids*, Vol. 18, No. 1, 2006, pp. 014103-14.

[30] Chedevergne, F., Casalis, G., and Majdalani, J., "Biglobal Linear Stability Analysis and DNS Investigation of the Flow Induced by Wall Injection," AIAA Paper 2007-5796, July 2007.

[31] Culick, F. E. C., and Yang, V., "Prediction of the Stability of Unsteady Motions in Solid Propellant Rocket Motors," *Nonsteady Burning and Combustion Stability of Solid Propellants*, Vol. 143, edited by L. De Luca, E. W. Price, and M. Summerfield, AIAA Progress in Astronautics and Aeronautics, Washington, DC, 1992, pp. 719-779.

[32] Culick, F. E. C., Burnley, V. S., and Swenson, G., "Pulsed Instabilities in Solid-Propellant Rockets," J*ournal of Propulsion and Power*, Vol. 11, No. 4, 1995, pp. 657-665.

[33] Flandro, G. A., "Effects of Vorticity on Rocket Combustion Stability," *Journal of Propulsion and Power,* Vol. 11, No. 4, 1995, pp. 607-625.

[34] Flandro, G. A., "Energy Balance Analysis of Nonlinear Combustion Instability," *Journal of Propulsion and Power*, Vol. 1, No. 3, 1985, pp. 210-221.

[35] Flandro, G. A., "Nonlinear Unsteady Solid Propellant Flame Zone Analysis," AIAA Paper 98-3700, 1998.

[36] Flandro, G. A., "On Flow Turning," AIAA Paper 952530, July 1995.

[37] Flandro, G. A., Cai, W., and Yang, V., "Turbulent Transport in Rocket Motor Unsteady Flowfield," *Solid Propellant Chemistry, Combustion, and Motor Interior Ballistics*, Vol. 185, edited by V. Yang, T. B. Brill, and W.-Z. Ren, AIAA Progress in Astronautics and Aeronautics, Washington, DC, 2000, pp. 837-858.

[38] Flandro, G. A., Majdalani, J, and Sims, J. D., "On Nonlinear Combustion Instability in Liquid Propellant Rocket Engines," AIAA Paper 2004-3516, July 2004 .

[39] Flandro, G. A., Majdalani, J., and French, J. C., "Incorporation of Nonlinear Capabilities in the Standard Stability Prediction Program," AIAA Paper 2004-4182, July 2004.

[40] Flandro, G. A., Majdalani, J., and Sims, J. D., "Nonlinear Longitudinal Mode Instability in Liquid Propellant Rocket Engine Preburner," AIAA Paper 2004-4162, July 2004.

[41] French, J. C., and Majdalani, J., "Hydrodynamic Stability Analysis of Solid Rocket Motors with Arbitrary Grain Design" AIAA Paper 2007-5808, July 2007

[42] Levine, J. N., and Baum, J. D., "A Numerical Study of Nonlinear Phenomena in Solid Rocket Motors," *AIAA Journal*, Vol. 21, No. 4, 1983, pp. 557-564.

[43] Majdalani, J., "The Boundary Layer Structure in Cylindrical Rocket Motors," *AIAA Journal,* Vol. 37, No. 4, 1999, pp. 505-508.

[44] Majdalani, J., and Roh, T. S., "Vorticity Dynamics in Isobarically Closed Porous Channels. Part II: Space-Reductive Perturbations," *Journal of Propulsion and Power,* Vol. 17, No. 2, 2001, pp. 363-370.

[45] Majdalani, J., and Van Moorhem, W. K., “Improved Time-Dependent Flowfield Solution for Solid Rocket Motors,” *AIAA Journal,* Vol. 36, No. 2, 1998, pp. 241-248.

[46] Majdalani, J., Flandro, G. A., and Roh, T. S., “Convergence of Two Flowfield Models Predicting a Destabilizing Agent in Rocket Combustion,” *Journal of Propulsion and Power,* Vol. 16, No. 3, 2000, pp. 492-497.

[47] Yang, V., and Roh, T. S., “Transient Combustion Response of Solid Propellant to Acoustic Disturbance in Rocket Motors,” AIAA Paper 95-0602, January 1995.

[48] Sirignano, W. A. and Crocco, L, “A Shock Wave Model of Unstable Rocket Combustion,” *AIAA Journal,* Vol. Vol 2, No. No. 7, 1964.

[49] Vyas, A. B. and Majdalani, J., “Asymptotic Temperature Distribution in a Simulated Combustion Chamber,” *Journal of Heat Transfer*, Vol. 129, No. 7, 2007, pp. 894-898.